H1-06/00-585

# Low $Q^2$ Physics and Runs

M. Klein, P. Newman and R. Wallny

7. 6. 2000

**Abstract:**

This note describes the physics interest and possible realization of dedicated data taking to complete the low $Q^2$ and low $x$ physics programme with $ep$ collisions at HERA with two short runs with shifted $z$ vertex position and reduced positron beam energy.

# 1 Introduction

In the nineties a remarkable amount of data has been recorded by H1 and ZEUS to study the kinematic region of low $Q^2$ and $x$ which opened the field of experimental, deep inelastic low $x$ physics. The observed rise of the structure function $F_2(x, Q^2)$ towards low $x$ implies that in future high energy accelerators (in particular at the LHC) quark-gluon interactions are to be described in the region of very large parton densities where the application of DGLAP perturbative QCD becomes doubtful. It remains one of the key tasks at HERA to not only provide high accuracy data for QCD parton densities but also to clarify their range of applicability. Despite ingenuitive theoretical efforts [1] this has not been achieved yet, and a new, modified field theoretical description of deep inelastic scattering at low $x$ could not yet be established.

It turns out that the $Q^2$ region around 1 GeV$^2$ is of particular interest as here the transition from soft to hard physics or from photoproduction to deep inelastic physics takes place. In this region higher order logarithmic (NNLO) and power corrections (higher twists) are very large and need to be accessed experimentally and mastered theoretically. Progress in this field depends on precision measurements of the structure function $F_2$ and its derivative $\partial F_2/\partial \log Q^2$as well as on complementary data of heavy flavour production and of diffractive processes. Of particular interest is the longitudinal structure function $F_L(x, Q^2)$ which permits QCD to be tested at higher orders and independently of $F_2$ . Moreover, $F_L$ is particularly sensitive to higher twist effects at low $Q^2$ and $x$ which have not been revealed yet.

So far the $Q^2$ region between 0.5 GeV$^2$ and 2 GeV$^2$ has been partially accessed in inclusive $ep$ cross section measurements at HERA by means of shifted vertex data of rather limited accuracy or with edge bins of nominal vertex data in a correspondingly limited range of $x$. It is argued that a new run with shifted vertex position towards $z = +70$ cm and in particular a run with lowered positron beam energy of $E_e \simeq 15$ GeV can yield rich and precise information which would complete the experimental programme of data taking at very low $x$ at HERA. It is estimated that such an experimental programme can be performed within three weeks of data taking. These runs may still and can only be performed during this year since after the luminosity upgrade superconducting magnets will be installed close to the interaction region. Those introduce an acceptance limitation of about $\theta_e \leq 173^o$ to the positron detection which corresponds to mimimum $Q^2$ values of roughly $Q^2 \simeq 10$ GeV$^2$ apart from the highest $y$ region.

This note is organized as follows. In Section 2 the present structure function data are shown and the completion of the kinematic range near $Q^2 = 0.01$ GeV$^2$ and around 1 GeV$^2$ is demonstrated for the shifted vertex run and for the low energy run. Section 3 presents the physics interest in further measurements at low $x$ and low $Q^2$ for some of the most important topics including a discussion of a possible measurement of $F_L$ . A brief summary is given in Section 4. The appendix describes the possible realization of a HERA run at reduced positron beam energy.

# 2 Inclusive Cross Section Data

## 2.1 Present Data of ZEUS and H1 on $F_2(x, Q^2)$ and $\sigma_{tot}^{\gamma^* p}$

Both collaborations have presented preliminary measurements of $F_2(x, Q^2)$ at low $Q^2$ with the main backward apparatus essentially based on the 1997 run [2, 3]. The data are consistent

with each other apart from a few % possible normalization difference. As can be seen in Figure 1 the low $Q^2$ region extending down to $Q^2 \simeq 2$ GeV$^2$ is measured rather precisely. This is apparent especially if one compares this data with the shifted vertex data shown in Figure 2, see below.

Another set of rather precise structure function data was published recently [4] by the ZEUS Collaboration in the $Q^2$ region between 0.1 and 0.65 GeV$^2$, with a few points at largest $y$ extending to $Q^2 = 0.045$ GeV$^2$. The H1 Collaboration took data in 1999 with their VLQ spectrometer covering a similar $Q^2$ range, between 0.1 and 0.4 GeV$^2$, which are being analyzed.

It is thus to be concluded that no precision data has yet been obtained for $Q^2$ between 0.5 and 2 GeV$^2$ at HERA since the accuracy of the pilot shifted vertex data is rather poor. Moreover there is no overlap of data taken with different detector systems which experimentally and for further analyses is disadvantageous. The presently reached minimum $Q^2$ in double differential cross section measurements is about 0.1 GeV$^2$ in a large range of $W$.

### 2.2 Shifted Vertex Data

In 1995 data with a vertex $z$ position shifted towards +70 cm were taken with a luminosity of about 0.1 pb$^{-1}$. The resulting structure function measurements [5, 6] are shown in Figure 2. The data extend to the region of low $Q^2$. Their accuracy is limited by statistics and systematics to about 10-15%.

The vertex shift changes the maximum angle of the scattered positron from $177^o$ to about $178^o$ for the main calorimeter and from $179.2^o$ to $179.4^o$ for the H1 very low $Q^2$ detector located at about $z = -3$ m. This leads to an extension into the lower $Q^2$ region as seen by the previous data and as illustrated in Figure 4. Shifted vertex running for the main apparatus leads to lower $Q^2$ but does not close the gap to the dedicated very low $Q^2$ spectrometer data. The acceptance gain towards lowest $Q^2$ for the VLQ is small for geometric reasons. Precision is achieved preferentially from running with nominal vertex position where detector acceptances and efficiencies are under control. Yet, the main advantage of a new shifted vertex run can be to obtain data in the main detector acceptance region of smallest $x$ for high $W$ which are not accessible with low energy running since $W \simeq \sqrt{sy}$.

### 2.3 Low Positron Energy Run

The main effect desired of lowering the positron beam energy regarding the low $Q^2$ region is that $Q^2$ diminishes by the ratio $(E_e/27.6)^2$ in a wide range of $x$ independently of $\theta_e$, i.e. with a run at 15 GeV one reduces the minimum $Q^2$ by a factor of 4. Thus the region between 2 and 0.5 GeV$^2$ can be fully covered, and the same gain is obtained for the very low $Q^2$ region, $Q^2 > 0.1$ GeV$^2$, contrary to the shifted vertex case. Thus the low energy run provides data with $Q^2$ significantly closer to the $\sigma_{tot}$ measurements making extrapolations of the $F_2$ data to $Q^2 = 0$ more reliable. The coverage of the kinematic plane with the low energy run is illustrated in Figure 5 to be compared with the coverage by shifting the vertex, Figure 4.

# 3 Physics Topics

## 3.1 DGLAP QCD Tests

Conventional tests of DGLAP QCD in inclusive $ep$ scattering at HERA are performed by fitting structure function data with parton distribution parametrizations starting at some initial scales $Q_0^2$. Typical examples are $Q_0^2$ around 0.5 GeV$^2$ in the GRV ansatz, about 1 GeV$^2$ as used by H1 for the fit presented at the Lepton-Photon Symposium in 1999 or 7 GeV$^2$ as used by the ZEUS Collaboration. The minimum $Q^2$ values for data included in these fits have a similar range. Often the fits are evolved backwards to describe data not used in the minimization. Regarding the region considered here a few peculiarities of these fits deserve particular attention:

- It has been seen that for $Q^2$ around 1 GeV$^2$ sea and gluon distributions follow a highly dynamic interplay. While common folklore tells that the derivative $\partial F_2/\partial \log Q^2$at low $x$ measures the gluon distribution, this does not hold in DGLAP QCD for $Q^2 \simeq 1$ GeV$^2$. In this region the gluon becomes valence like [7,8], and the rise of $F_2$ is due to the sea which then, at somewhat larger $Q^2$, exchanges this role with the gluon distribution $xg$. This is demonstrated in a plot taken from the 1998 MRST analysis [9] showing the two exponents $\lambda_S$ and $\lambda_g$, for $xq \propto x^{-\lambda}$, as a function of $Q^2$, see Figure 6. These interchange their role at $Q^2$ near 2 GeV$^2$.

- In determinations of the gluon distribution at low $x \leq 10^{-4}$ the data at very low $Q^2$ play a particularly crucial role as they are the main source of uncertainty of $xg$ which leads to the widened band of the gluon distribution at low $x$. This is illustrated in Figure 7 which presents two gluon distributions from two NLO DGLAP fits to the H1 data. Those differ only by the assumption of whether the data for $Q^2 \geq 1.5$ GeV$^2$ are included in the fit or only data for $Q^2 \geq 3.5$ GeV$^2$. Precision data near to $Q^2$ of 1 GeV$^2$ in the full range of $x$ are required in order to distinguish between a possible edge effect related to the lowest $x$ points and a different physics behaviour. Similar observations were made by the fits performed by the ZEUS collaboration [8].

- Surprisingly, DGLAP fits of this type can be extended down to very low $Q^2$ where $\alpha_s$ and $\log(1/x)$ are already larger than any perturbative expansion would permit [10].

- Very recent analyses suggest that the gluon distribution is subject to very large corrections in next-to-NLO pQCD [9]. At low $Q^2$ it is possible that the gluon becomes even negative (see Figure 8) though observables as the longitudinal structure function have to remain positive.

- With the gluon distribution vanishing at low $Q^2$, the charm structure function $F_2^c$ can be expected to be drastically reduced at low $x$ for $Q^2 \simeq 1$ GeV$^2$ which would be an independent test of the parton dynamics in the kinematic region under consideration.

All these observations demonstrate that in order to pin down the behaviour of the gluon density and to test the applicability of DGLAP QCD, data near 1 GeV$^2$ of highest possible precision are essential. The inclusive measurements have to include $F_2(x, Q^2)$, thereby its derivative $\partial F_2/\partial \log Q^2$, and also the longitudinal structure function $F_L(x, Q^2)$, see below.

### 3.2 The derivative $\partial F_2/\partial \log Q^2$ and the photoproduction limit $Q^2 \simeq 0$

A quantity of particular interest is the derivative $\partial F_2/\partial \log Q^2$ which gave rise to crucial tests of QCD since the analysis of BCDMS structure function data in the eighties. With the presentation of the turnover behaviour of a one-dimensional derivative $dF_2/dlogQ^2$, essentially along the region of constant $y$ and averaging over $y$, the derivatives of $F_2$ based on HERA data became subject to an intense, fruitful discussion between theorists and experimentalists [12]. Figure 9 shows the recent two-dimensional measurements of $\partial F_2/\partial \log Q^2(x, Q^2)$ by H1 [2] and by ZEUS [13] in bins of $Q^2$ [1]. An analysis of the H1 data based on the GRV structure function parametrization lead to the suggested observation of screening corrections at low $x$, see Figure 9, although this derivative is also described by the H1 NLO DGLAP fit without any additional correction, see [2]. The recent analysis of $\partial F_2/\partial \log Q^2$ by the ZEUS collaboration included low $Q^2$ data from the BPT detector and also fixed target data extending beyond and partially interpolating in the HERA kinematic range. The data, when plotted at fixed $W$, exhibit a similar characteristic shape versus $Q^2$ as the previously considered one-dimensional quantity $dF_2/dlogQ^2$ [14].

From a naive dipol model ansatz [18], using a few parameter description of $F_2$ , $F_L$ and also of diffractive scattering, a region is derived where saturation may set in. This is expected to happen where the transverse dipole extension and the proton target are of about equal size. As can be seen in Figure 10 this line is just in the $(Q^2, x)$ region under discussion here where precision data are lacking.

Extension of the very recent derivative analysis of the ZEUS Collaboration with low energy run data approaching $Q^2 > 0.02$ GeV$^2$ can complete the picture of the behaviour of $\partial F_2/\partial \log Q^2$ at fixed $W$ at extremely low $Q^2$. While this is of interest, a more direct question regards the cross section behaviour itself. As can be seen in Figure 5 the low energy run leads to data down to $Q^2$ of 0.02-0.03 GeV$^2$ for a wide range of $W$. This will enable clarification whether the $F_2$ data extrapolated to $Q^2 \simeq 0$ are fully consistent with possibly improved measurements of $\sigma_{tot}$ or remain to be above those as had been indicated by the extrapolation of ZEUS data [16], see Figure 11.

### 3.3 Measurement of $F_L(x, Q^2)$ and Higher Twists

The envisaged run at reduced positron beam energy permits the longitudinal structure function $F_L$ to be measured, independently of assumptions about $F_2$ . A simultaneous systematic study of $F_L(x, Q^2)$ and $F_2(x, Q^2)$ allows the issue of mixing of small and large distances to be disentangled in a much more accurate way than may be achieved by studying $F_2(x, Q^2)$ alone. A measurement of $F_L$ for $Q^2 \sim 2$ GeV$^2$ is in a particularly interesting range. It corresponds to the region of rather small interquark distances $b \sim 0.4$ fm where pQCD predicts a fast growth which is markedly different from $F_T$ where much larger distances dominate. At the same time in the covered region of smallest $x$ one is close enough to the unitarity limit and hence the growth could start to be tamed [17].

[1] Note that the derivatives in this representation are based on approximate, quadratic expressions of $F_2$ vs. $\log Q^2$. The errors therefore are to a large extent driven by the range of fitting of $F_2$. While this range for H1 is restricted to H1 data with $Q^2 \geq 2$ GeV$^2$, for ZEUS it includes their BPT lower $Q^2$ data and also the E665 and NMC data, thus a much wider range in $\log Q^2$ is fitted. The local derivatives, based on adjacent bins in $Q^2$ at fixed $x$ for the H1 experiment were presented at the 1999 Lepton-Photon Symposium at SLAC.

The numerical size of the non-perturbative contribution, neglected in the standard perturbative QCD formulae for $F_L(x,Q^2)$ and $\partial F_2/\partial \log Q^2$, may be pinned down by studying the relative and absolute $x$ and $Q^2$ dependence of these two quantities. The effect of higher twist corrections to $F_L(x,Q^2)$ is predicted to be very large [18], changing the prediction by a factor of about two in the region of possible measurements of $F_L(x,Q^2)$. This is illustrated in Figure 4 obtained from [19].

The kinematic range of this measurement is visualized in Figure 13. It is limited at low $Q^2$ by the maximum $\theta_e$ accepted in standard run conditions and at high $Q^2$ by the minimum $\theta_e$ which for H1 is a range between about $176.5^o$ and $155^o$. The lower acceptance limit is removed if the shifted vertex data are compared with the low energy run data. Thus one would obtain data on $F_L$ below $Q^2 \simeq 1$ GeV$^2$ with statistical meaningful accuracy. Since the systematic accuracy of such a data set combination is difficult to assess, it has not been considered any further in the present simulation of the $F_L$ measurement. Yet, it may deserve attention.

The accuracy of the $F_L(x,Q^2)$ measurement depends on the maximum $y$, i.e. the minimum scattered positron energy one can reliably access. In the case of the H1 measurement Silicon tracking, high resolution calorimetry and a special trigger based on tracks and energy deposition permit the cross section to be measured with high efficiency down to $E'_e$ of 3 GeV corresponding to a maximum $y$ of 0.8 for 15 GeV incoming energy. Assuming a systematic error of 4-3%, as obtained for the 1997 data analysis for $y$ between 0.8 and 0.5, and using luminosities of 3 pb$^{-1}$ for standard running and of 0.5 pb$^{-1}$ for the low energy data, the statistical and systematic accuracy of the $F_L$ measurement has been estimated. The result is given in Figure 14. As can be seen the measurement is systematics dominated at lowest $Q^2$. Yet, no less than 0.5 pb$^{-1}$ of low beam energy data should be available for analysis.

The largest uncertainty in the present analyses of high $y$ data is due to photoproduction background. This becomes less pronounced at 15 GeV since the incoming energy changes the kinematics of the photoproduction background in a favourable way. This is demonstrated in Figure 15 which compares the energy distributions of simulated events in PHOJET for 27.6 GeV and 15 GeV positron beam energies. The kinematics scales about in $y$ and affects the angular and the scattered energy distributions. This plot suggests that handling the photoproduction background at fixed scattered energy is expected to be easier for the low energy run as compared to nominal running, i.e. one may not just scale the high $y$ limits but consider to be able to obtain reliable data at lower energy of the scattered positron in the 15 GeV run than in the 27.6 GeV run. This is particularly interesting for an experimental arrangement with less powerful tracking in front of the calorimeter as, for example for H1, at very large angles below the acceptance of the backward silicon tracker BST.

While the $F_L$ data at lowest $Q^2$ can only be obtained now, the measurement of $F_L(x,Q^2)$ at larger $Q^2$ [20] can be deferred to the high statistics phase of HERA when taking a series of runs, likely then with reduced proton beam energies, will be less time consuming than presently.

### 3.4 Diffraction and Vector Meson Production

The importance of data at low $Q^2 \sim 1$ GeV$^2$ is not restricted to the inclusive cross section. It concerns dijet data, for example the relative importance of hadronic (non-perturbative) and

perturbative components of photon structure and their dependence on $Q^2$, and heavy flavour production at small $Q^2$.

In diffraction the transition from hard to soft physics is particularly striking. The $W$ dependence of the photoproduction measurement is consistent with the soft pomeron universally describing hadronic total, elastic and dissociation cross sections [21]. The result in the deep-inelastic regime is not. The transition region therefore deserves precision measurements. Theoretical models based on different dynamical assumptions for diffractive DIS give varying predictions for the energy (or $1/x$) dependence of the ratio $F_2^D/F_2$ and how it should vary with $Q^2$.

Another example briefly worth mentioning is the production of vector mesons. Their cross sections are very large at low $Q^2$ (e.g. the elastic $\rho$ cross section is around 10% of the total photoproduction cross section but is then suppressed like $1/Q^2$ compared to standard DIS). The proposed data samples would have very high $\rho$ and $\phi$ yields in particular, allowing high precision measurements to be made.

An increase with $Q^2$ of the effective pomeron intercept $\alpha_{I\!P}(0)$ governing $\rho$ production has recently been observed in the region $Q^2 = 1$ GeV$^2$ [22]. It is very interesting to compare this variation with that observed for $F_2$ and for $F_2^D$ to help distinguish between models as discussed in the context of diffractive dissocation.

The recently observed violation of s-channel helicity conservation (SCHC) for the $\rho$ at large $Q^2$ [22] has been successfully reproduced in models based on pQCD [23]. The dependence of the SCHC violation on $Q^2$ and $|t|$ is clearly predicted in such models. Measurements of the full set of spin density matrix elements in as wide a kinematic range as possible are clearly desirable in order to test this significant advance in the boundaries of our understanding of QCD.

We also measure absolute cross sections, $t$ slopes, $\rho$ lineshape skewing and the ratio $\sigma_L/\sigma_T$ as a function of $Q^2$. ZEUS BPC data [22] for the $\rho$ at $Q^2 \sim 0.5$ GeV$^2$ have given the first hint as to how all of these observables approach the photoproduction limit. Measurements in additional $Q^2$ regions and for different vector meson species are crucial to our understanding of vector meson production and higher twist processes in general in QCD.

# 4 Summary

With two additional runs, by shifting the $z$ vertex position by +70 cm and by reducing the positron beam energy to about 15 GeV, the HERA low $Q^2$ and $x$ data taking and analysis programmes can be completed. These runs will lead to partially complementary data sets covering the low $Q^2$ region around 1 GeV$^2$ where precision data from HERA are missed. This is the region of predicted saturation, of very high NNLO corrections in DGLAP QCD, of large higher twist corrections to $F_L$, of a dynamic interchange of the role of sea and gluon distributions in the proton and of the low $x$ transition from soft to hard processes. A physics programme has been sketched requiring precision data on $F_2(x,Q^2)$ and $\partial F_2/\partial \log Q^2$and a measurement of $F_L(x,Q^2)$. This data set will be of much use for diffractive, vector meson, dijet and also heavy flavour physics studying similar questions in a less inclusive but complementary way. Luminosities of at least 0.5 pb$^{-1}$ are required for the shifted vertex and for the low energy run. Given HERAs present run conditions and past experience it is expected

that the shifted vertex data taking can proceed in a few days. As estimated in the appendix, at 15 GeV an amount of 0.5 pb$^{-1}$ of luminosity can be obtained within one week of running requiring in addition 10-14 days of set-up time for this initial run with reduced lepton beam energy. The whole programme can thus be performed within about three weeks of data taking. It has to be realized during the run 2000 since the luminosity upgrade will exclude the low $Q^2$ region of H1 and ZEUS. This is indeed the last moment to review and still improve the low $Q^2$ measurements at HERA.

## Acknowledgements

Stimulating discussions are acknowledged with J. Bartels, J. Blümlein, M. McDermott, K. Golec-Biernat, E. Levin, K. Peters, R. Roberts, S. Schlenstedt, M. Strikhman, A. Vogt, R. Yoshida and many members of the H1 Collaboration.

## A Running at Low Positron Beam Energy [2]

If the lepton beam energy $E_0$ is reduced to $E$, the lepton beam emittance is reduced as $\epsilon \propto (E/E_0)^2$. HERA colliding beam experience tells us that the beam sizes for leptons and protons must be kept matched. Therefore the emittance change has to be balanced by increasing the $\beta$-function of the leptons as $\beta/\beta_0 \propto (E_0/E)^2$ . This would increase the beam-beam tune shift of the leptons by a factor $(E_0/E)^3$ since that is proportional to $\beta$ and $1/E$. In addition, the maximum beam-beam tune shift reduces with the damping time. According to experience of running PETRA in $e^+e^-$ collisions at various energies, this reduction is expected to be proportional to $E_0/E$. To avoid that the leptons suffer from intolerable beam-beam effects, the proton beam current must be reduced by a factor $(E_0/E)^4$.

There is another effect causing a problem: The bunch length decreases linearly with energy $\sigma_s \propto E/E_0$. This leads to enhanced HOM heating of the H1 beam pipe which is not tolerable. The dissipated power is $P \propto I_e^2/\sigma_s$. This is also confirmed by measurements of temperatures at the collimator of the H1 beam pipe. If a beam current of 40mA is stored at 12 GeV, the temperature rises above $80^o$ C (equilibrium has never been reached so far). If this beam is accelerated to 27.5 GeV, the temperature drops to $40 - 60^o$ C and then decays further with decaying beam current. A somewhat pessimistic estimate is a roughly linear decrease of the dissipated power with beam energy. Thus the lepton current should be reduced by a factor $(E/E_0)^{0.5}$. Combining the beam-beam tuneshift consideration and the beam pipe heating effect, one expects that the luminosity will be reduced proportional to $L = L_0 \cdot (E/E_0)^{4.5}$.

This can be improved by changing the focusing in the arcs from presently $60^o$ $\beta$-tron phase advance per FODO cell to weaker focusing which gives larger beam emittance for the same energy. The lepton emittance varies with the phase advance per FODO cell $\Delta\Phi$ like $\epsilon \propto (\Delta\Phi_0/\Delta\Phi)^3$.

Another measure is a change in the damping distribution. By an rf frequency shift, the leptons are forced to an off-momentum orbit which passes off-centre of the quadrupole

[2] This part is due to F.Willeke [24].

| Parameters | Leptons | Proton |
|---|---|---|
| energy/GeV | 15 | 920 |
| damping distribution number | D=-0.5 | |
| phase advance $\Delta\Phi$ /FODO cell | $\pi/4$ | $\pi/2$ |
| beam current/mA | 27.1 | 42.0 |
| particles per bunch | $1.896 \cdot 10^{10}$ | $3.079 \cdot 10^{10}$ |
| number of bunches | 189 | 180 |
| beam emittance/nm | $\epsilon_x = 55.008$ | $\epsilon_{xn}(\gamma_p 4)^{-1} = 4.079$ |
| $\beta_x$/m | 0.709 | 7 |
| $\beta_y$/m | 0.425 | 0.5 |
| hor. BB tuneshift parameter | $\Delta\nu_x = 0.009$ | $\Delta\nu_x = 6.792 \cdot 10^{-4}$ |
| ver. BB tuneshift parameter | $\Delta\nu_y = 0.021$ | $\Delta\nu_y = 1.981 \cdot 10^{-4}$ |

Table 1: *Machine parameters for 15 GeV running. The resulting peak luminosity is* $4.5 \cdot 10^{30}\ cm^{-1}s^{-1}$ *which represents a factor of 3.9 reduction as compared to nominal energy running.*

magnets. This changes the balance between longitudinal and transverse damping which is expressed by a dimensionless damping distribution parameter $D$. $D$ is zero in the nominal case $D_0 = 0$. A change in $D$ is expected to be limited to values of approximately $|D| = 0.5$ due to closeness to the damping pole (where anti-damping sets in) and dynamic aperture effects. However, an increase of transverse beam emittance by this effect reduces the bunch length and vice versa. A change in the damping distribution $D$ which changes the bunch length as $\sigma_s \propto \sqrt{1 - D_0}/\sqrt{1 - D}$ will change the beam emittance by $\epsilon \propto (1 + D_0)/(1 + D)$.

We expect, that the $\beta$-tron phase advance per FODO cell could be as low as $\Delta\Phi = 45^o$. Assuming further that the damping distribution is changed from $D_0 = 0$ to $|D| = 0.5$, a luminosity of $L = 1.6 \times 10^{30} cm^2 sec^{-1}$ can be obtained at a lepton beam energy of 12 GeV which rises to $L = 4.5 \times 10^{30} cm^2 sec^{-1}$ at $E_e = 15$ GeV. The parameters for collisions of 15 GeV leptons are given in Table 1. Including an estimated setup time of 10-14 days, an initial low positron energy run at 15 GeV with a luminosity of 0.5 $pb^{-1}$ requires about three weeks.

# References


[1] For a recent review see: W. Van Neerven, *Deep-Inelastic Lepton-Hadron Scattering as a Test of Perturbative QCD*, Invited Talk at DIS'99, Zeuthen, April 1999, hep-ph/9905503, Proceedings of DIS'99, Nucl. Phys. **B 79** Proc. Suppl. (1999), ed. by J. Blümlein and T. Riemann.

[2] H1 Collaboration, M. Klein, Talk at the Lepton-Photon Symposium 1999, SLAC , hep-ph/0001059 (2000).

[3] ZEUS Collaboration, N. Tuning, Talk at DIS 2000, Liverpool, April 2000.

[4] ZEUS Collaboration, DESY 00-071 (2000), hep-ex/0005018.

[5] ZEUS Collaboration, M. Derrick et al., Z. Phys. **C 72** (1996) 399.

[6] H1 Collaboration, C. Adloff et al., Nucl. Phys. **B 497** (1997) 3.

[7] H1 Collaboration, A Measurement of the Inclusive Deep Inelastic $ep$ Scattering Cross Section at Low $Q^2$ at HERA, paper submitted to the EPS Conference Jerusalem 1997.

[8] J. Breitweg et al., ZEUS Collaboration, Eur. Phys. J. **C 7**, 609 (1999).

[9] A. D. Martin et al., Phys. Lett. **B443** (1998) 301.

[10] M. Botje, Contribution to the low $x$ Workshop, Zeuthen 1998.

[11] R. G. Roberts, Talk presented at DIS2000, Liverpool, April 2000.

[12] A. Caldwell, Inv. Talk, DESY Theory Workshop, Hamburg, October 1997.

[13] B. Foster, Talk at the Royal Society, 23.5.2000;

[14] R. Yoshida, ZEUS Collaboration, private communication.

[15] E. Levin, Talk presented at DIS2000, Liverpool, April 2000.

[16] C. Amelung, ZEUS Collaboration,Contribution to DIS99 Zeuthen, Proceedings, Nucl. Phys. **B79** (1999) 176.

[17] M. Mc Dermott and M. Strikhman, private communication.

[18] K. Golec-Biernat and M.Wüsthoff, Phys.Rev. **D59** (1999) 014017.

[19] K. Peters and K. Golec-Biernat, private communication.

[20] L. Bauerdick, A. Glazov and M. Klein, *Future Measurement of the Longitudinal Proton Structure Function at HERA*, Workshop on Future Physics at HERA, eds. G. Ingelmann, A. deRoeck and R. Klanner, Hamburg, DESY (1996), p.77.

[21] A. Donnachie, P. Landshoff, Phys. Lett. **B296** (1992) 227.

[22] ZEUS Collaboration, Eur.Phys.J. **C 6** (1999) 603.
H1 Collaboration, Eur.Phys.J. **C 13** (2000) 371.

[23] D. Ivanov, R. Kirschner, Phys Rev **D 59** (1998) 114026.

[24] F. Willeke, "HERA luminosity with reduced lepton beam energy", in preparation.

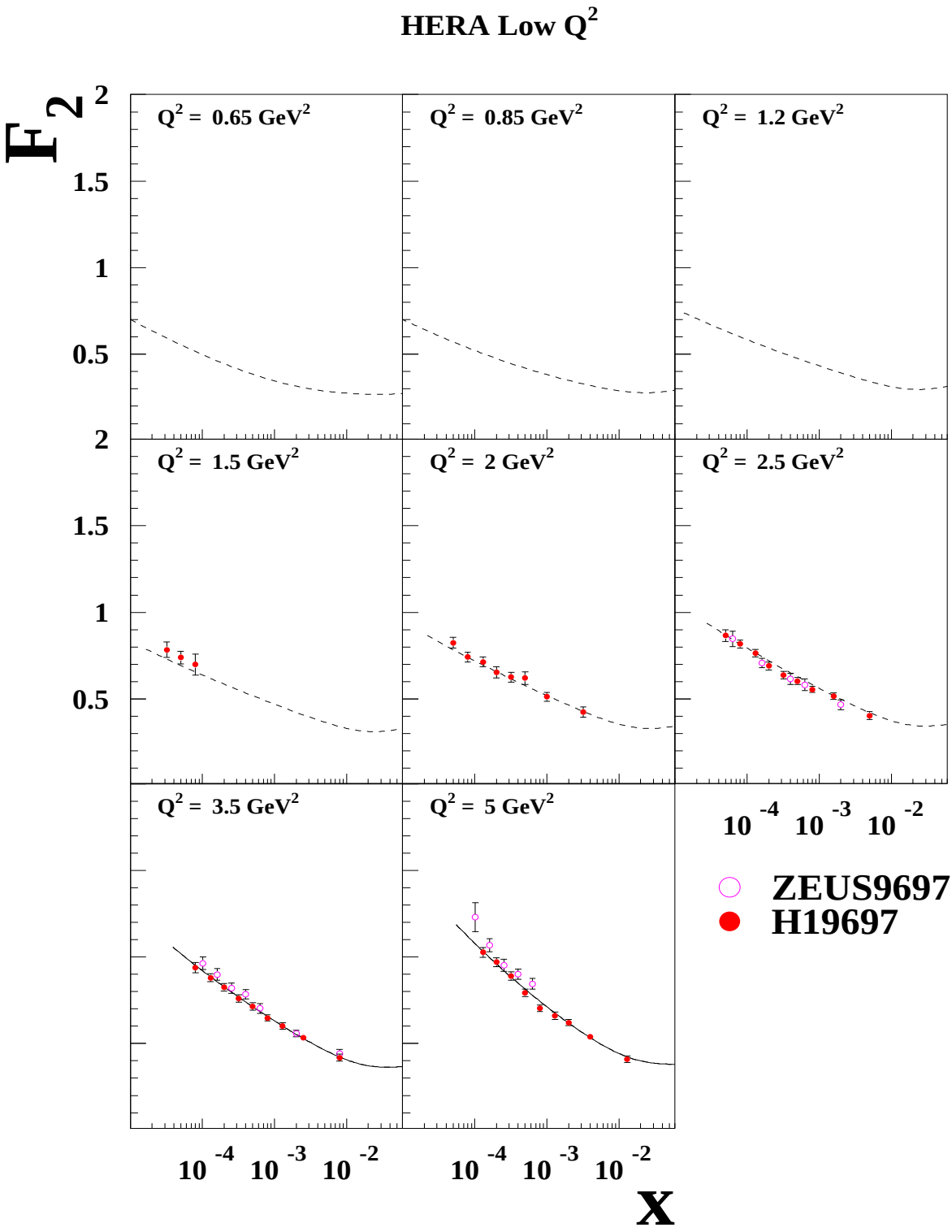


Figure 1: Preliminary measurements of the structure function $F_2(x, Q^2)$ by H1 and ZEUS with the standard backward apparatus extending in acceptance to about 176-177$^o$, corresponding to full acceptance for $Q^2 \geq 2.5$ GeV$^2$. In this region the precision of the data is a few %. The lines represent the NLO DGLAP QCD fit to the H1 data with a minimum $Q^2$ of 3.5 GeV$^2$, they are dashed in the range below.

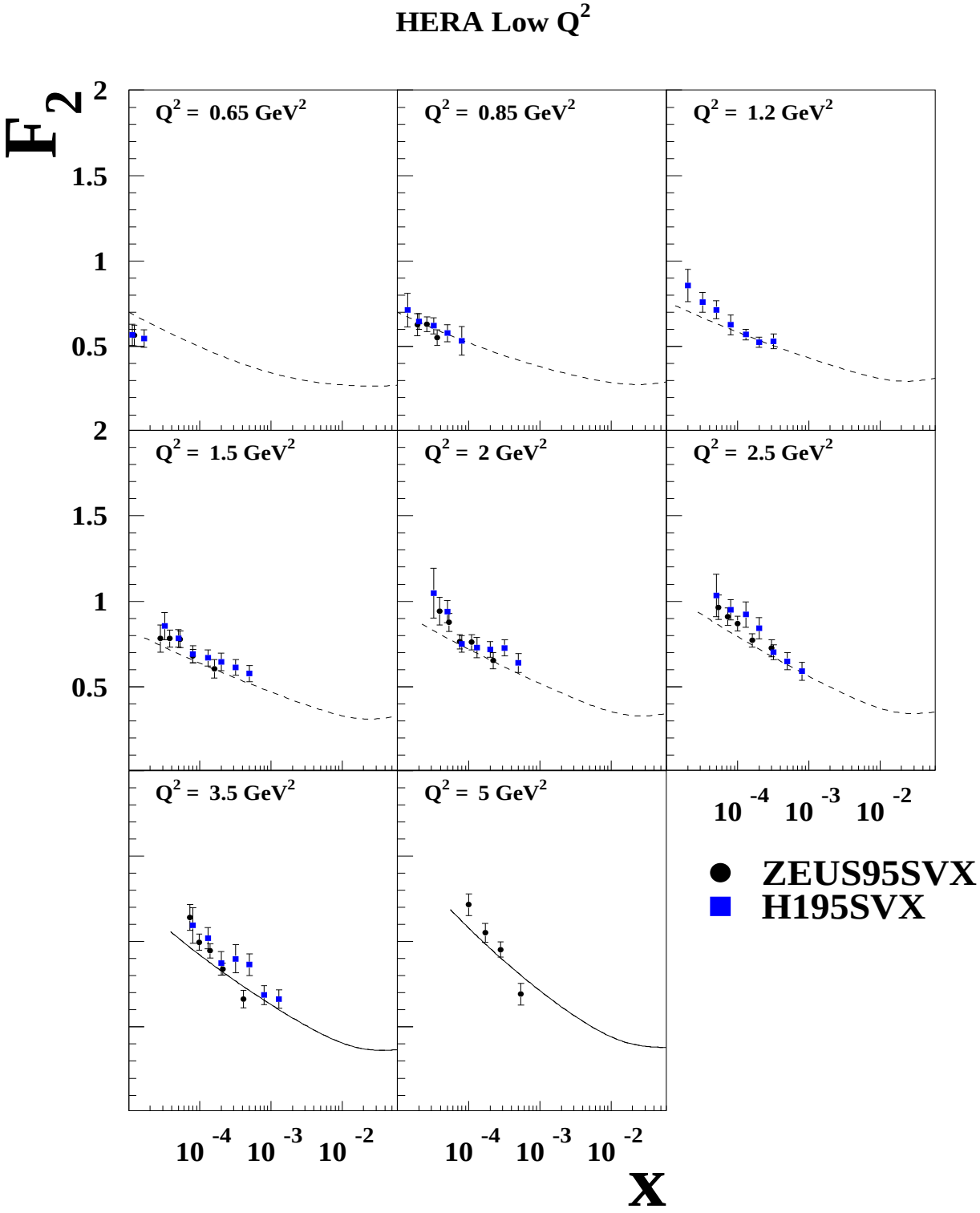


Figure 2: Measurements of the structure function $F_2(x, Q^2)$ by ZEUS and H1 taken in 1995 with shifted vertex position. The accuracy of the data is about 10%, and they tend to be higher than the nominal vertex data in the region of overlap, compare the previous figure. The lines represent the NLO DGLAP QCD fit to the preliminary nominal vertex H1 data with a minimum $Q^2$ of 3.5 GeV$^2$, they are dashed in the range below.

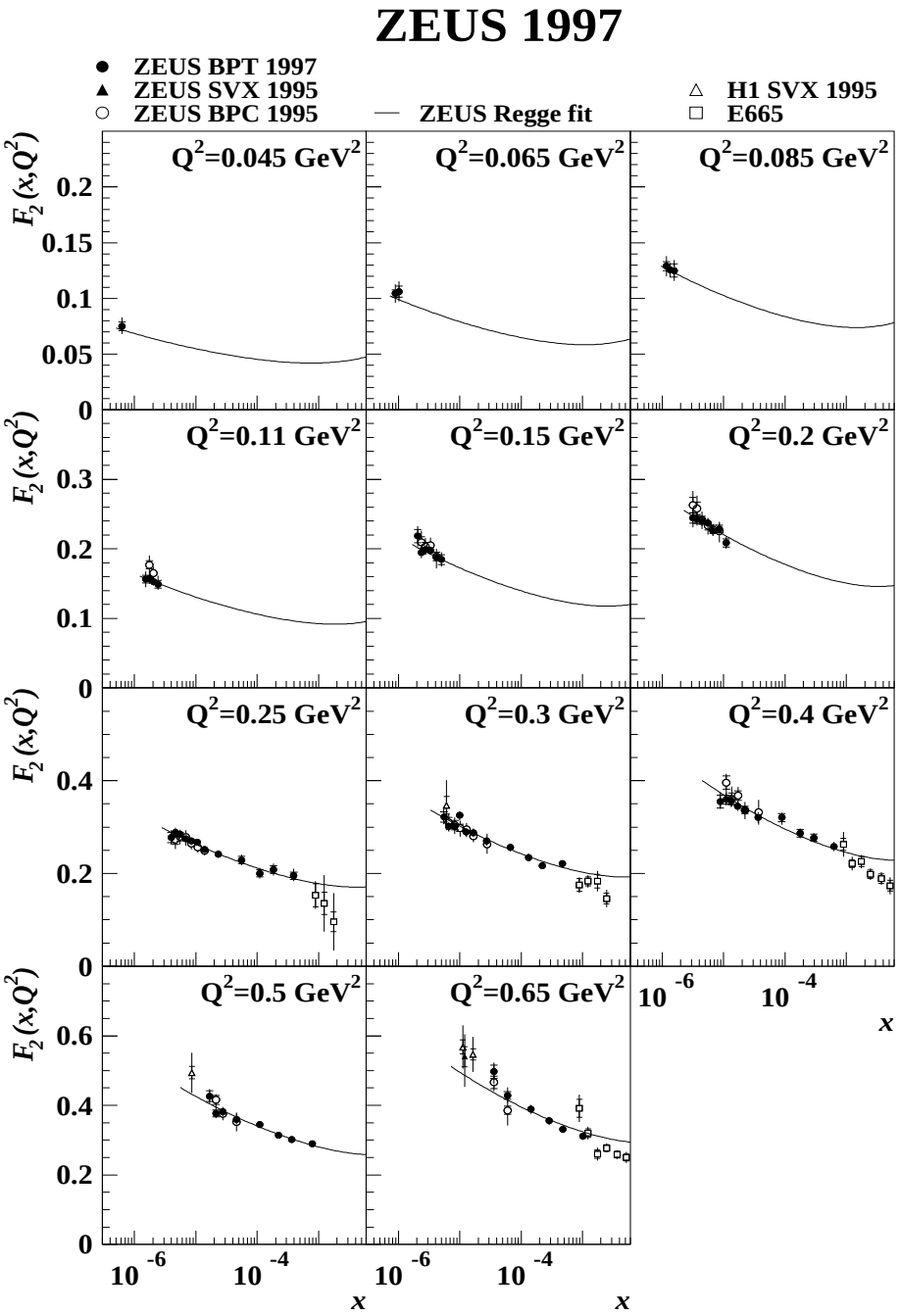


Figure 3: Measured $F_2$ vs. $x$ in bins of $Q^2$. The data from the present measurement are indicated by filled circles. The solid line shows the ZEUS Regge fit. Open circles denote the results from a previous analysis, filled and open triangles denote other measurements from ZEUS and H1, respectively, and squares denote results from E665. These other measurements have been shifted to the $Q^2$ values of the present measurement using the ALLM97 parameterization. The inner error bars represent statistical errors, the outer ones the sum in quadrature of statistical and systematic errors; normalization uncertainties are not included.

Figure 3:

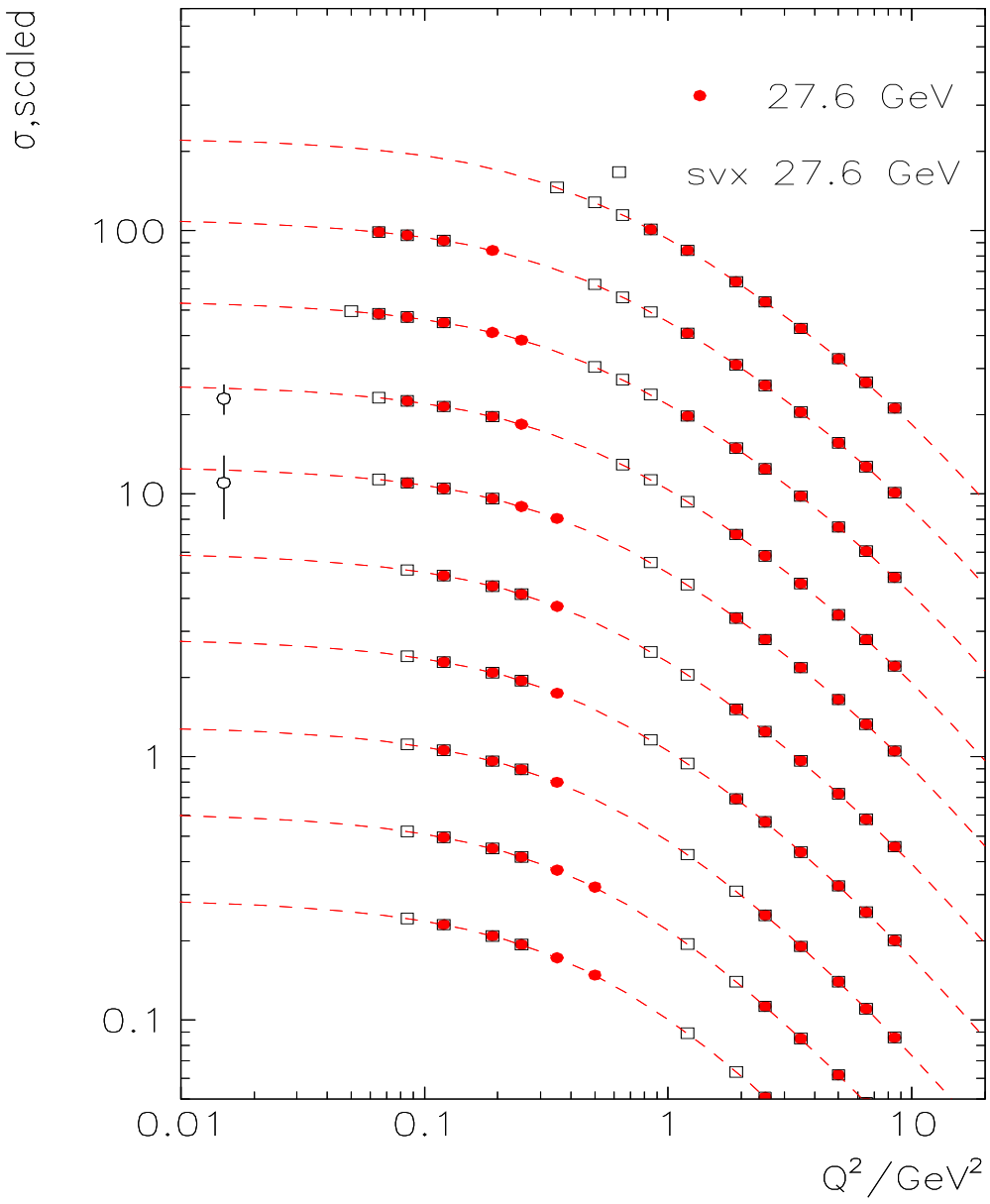


Figure 4: Simulated measurement of the virtual photon-proton interaction cross section for 920 GeV standard running (closed points) and shifted vertex running (open squares). The two sets of data at lowest and higher $Q^2$ correspond to the VLQ and SPACAL calorimeter acceptances with Silicon tracking in front, respectively. The two data points at lowest $Q^2$ denote the measurements of the total photoproduction cross section at $W = 172$ GeV and at $W = 189$ GeV arbitrarily plotted at the lowest visible $Q^2$ edge in this plot. The points represent simulated data with increasing $W$ for $W = 35., 50., 70., 100., 130., 172., 189., 220., 240., 260.$ GeV. The statistical errors are below the symbol size.

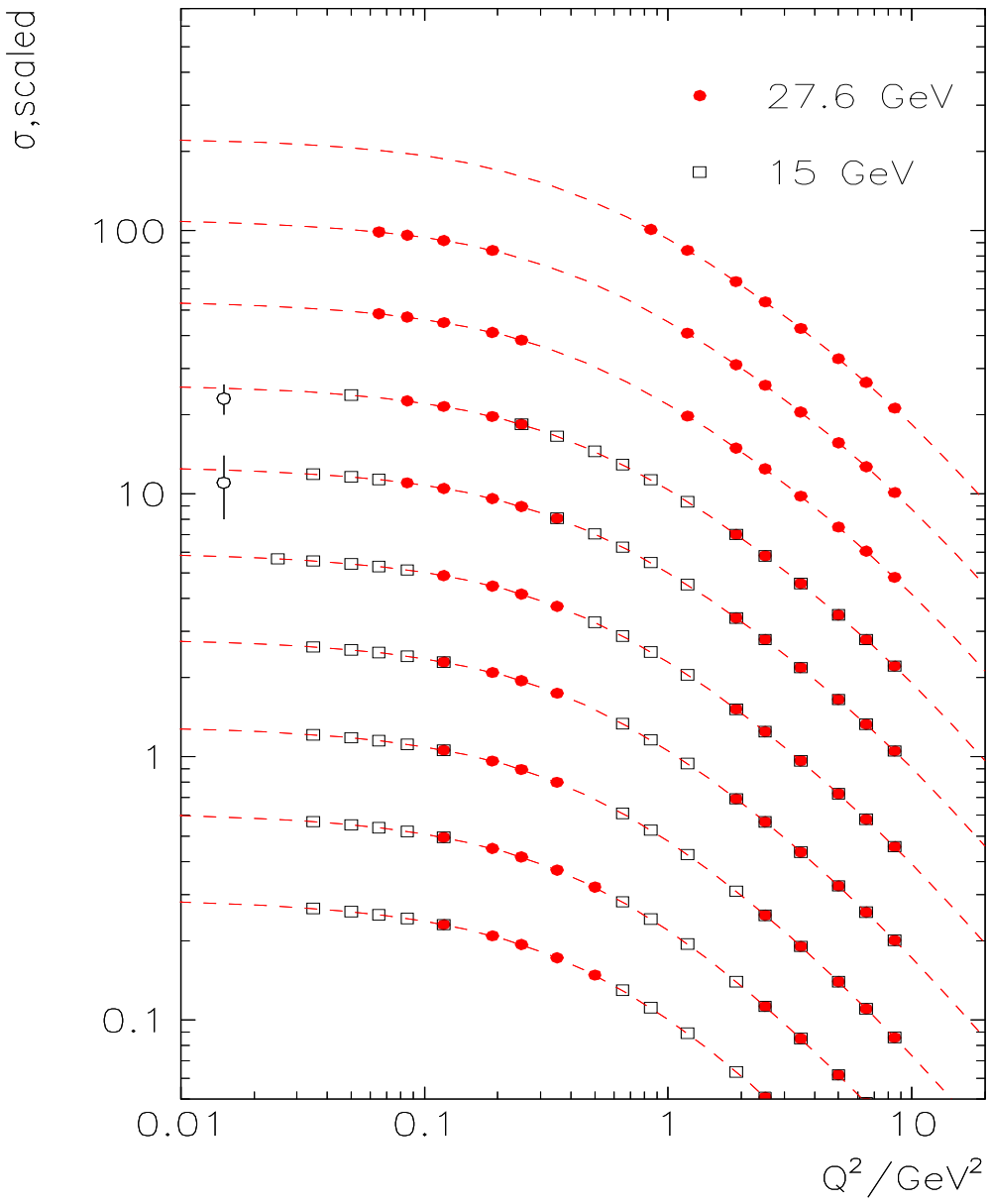


Figure 5: Simulated measurement of the virtual photon-proton interaction cross section for standard running (closed points) and low energy running (open squares). The two sets of data at lowest and higher $Q^2$ correspond to the VLQ and SPACAL calorimeter acceptances with Silicon tracking in front, respectively. The two data points at lowest $Q^2$ denote the measurements of the total photoproduction cross section at $W = 172$ GeV and at $W = 189$ GeV arbitrarily plotted at the lowest visible $Q^2$ edge in this plot. The points represent simulated data with increasing $W$ for $W = 35., 50., 70., 100., 130., 172., 189., 220., 240., 260.$ GeV. The statistical errors are below the symbol size.

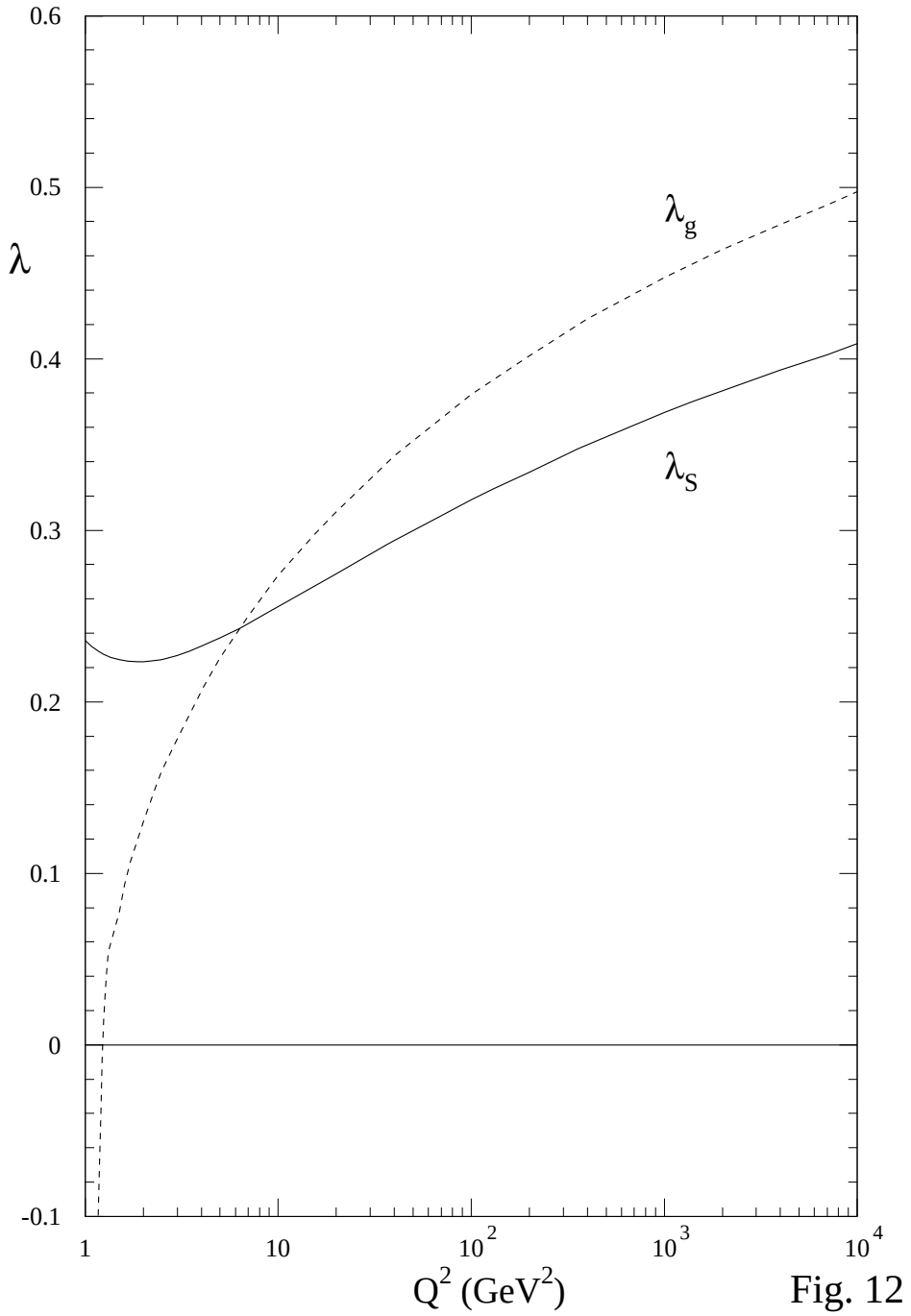


Figure 6: $Q^2$ dependence of the exponents $\lambda$ of the sea and the gluon distributions parametrized at low $x$ as $xq \propto x^{-\lambda}$ in a recent DGLAP QCD parton distribution analysis by the MRST group. Notice the huge dynamics interchange between gluon and sea for $Q^2$ between 1 and 3 GeV$^2$.

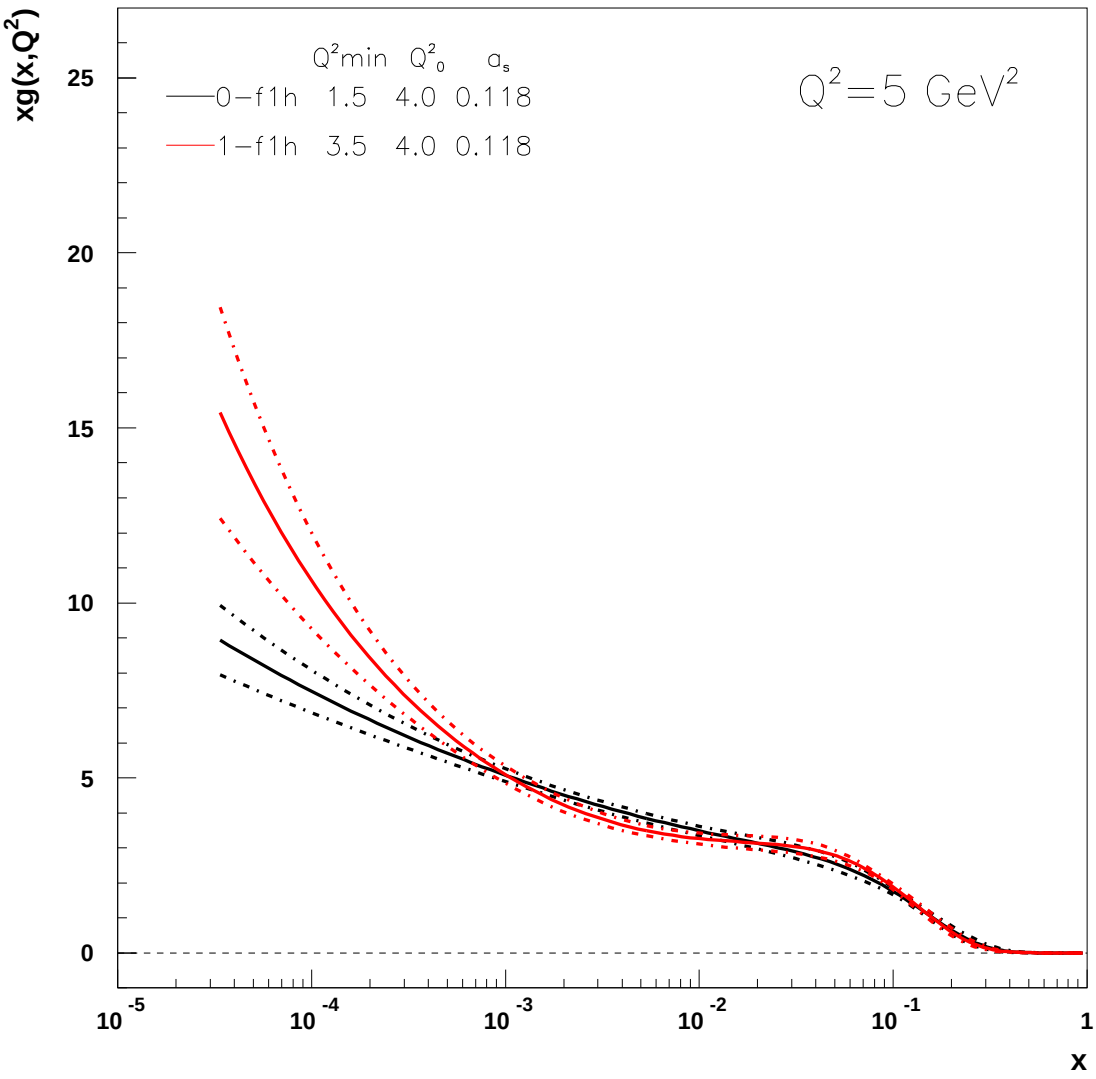


Figure 7: Gluon distributions determined with two NLO QCD fits to the H1 data. The fits differ by the $Q^2_{min}$ value considered which leads to a rather flat or a rather steep gluon at $Q^2 = 5$ GeV$^2$.

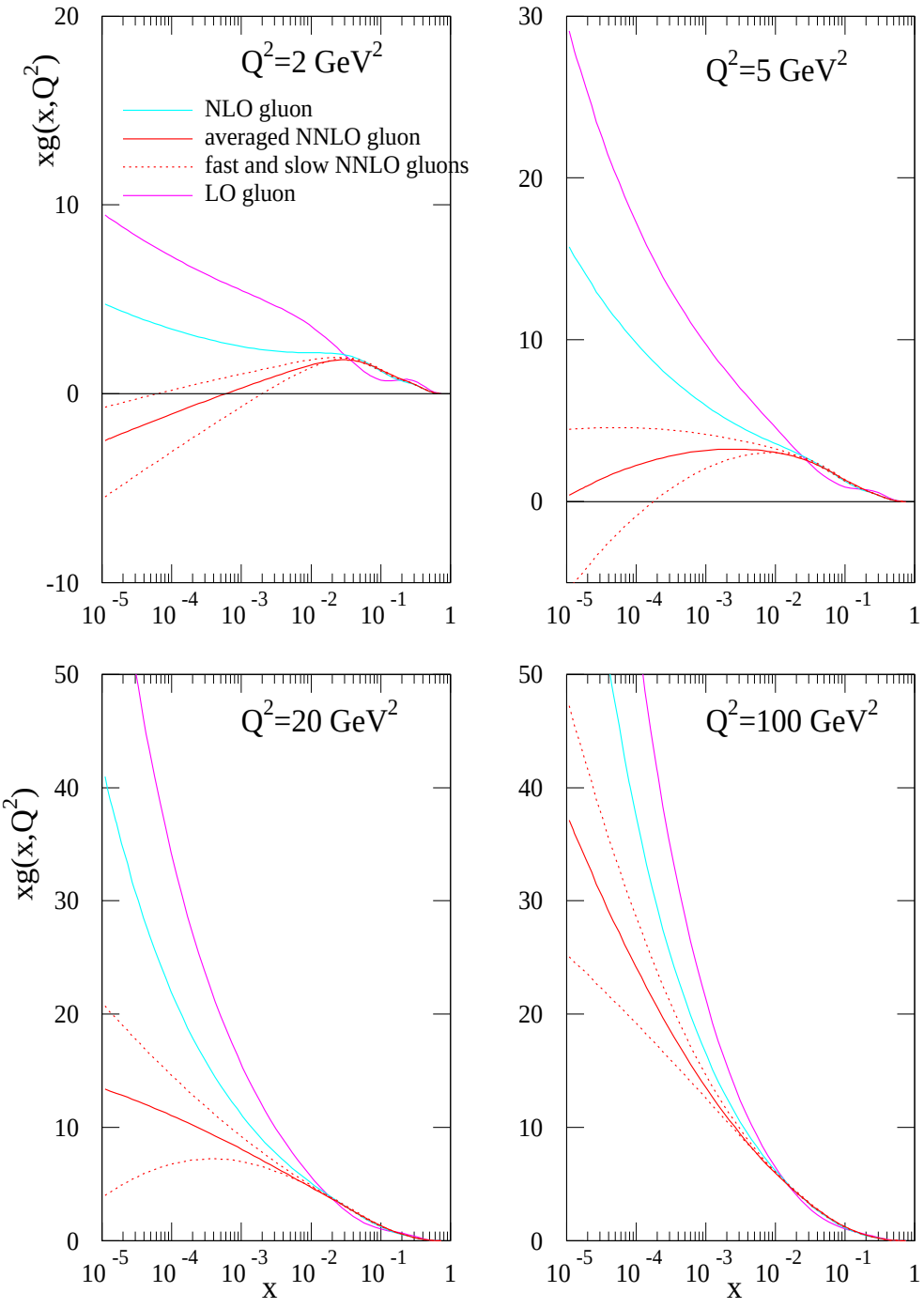


Figure 8: Calculations of the gluon distribution in DGLAP QCD to different orders as presented recently [11]. At low $Q^2$ the gluon distribution is seen to receive large contributions from NNLO corrections which may lead to a negative density.

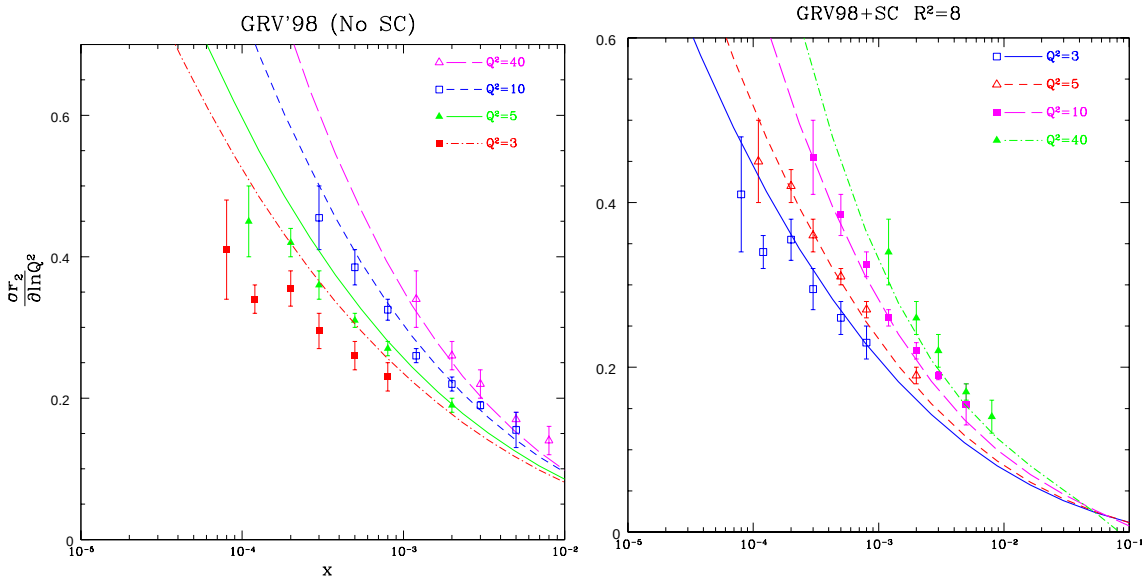


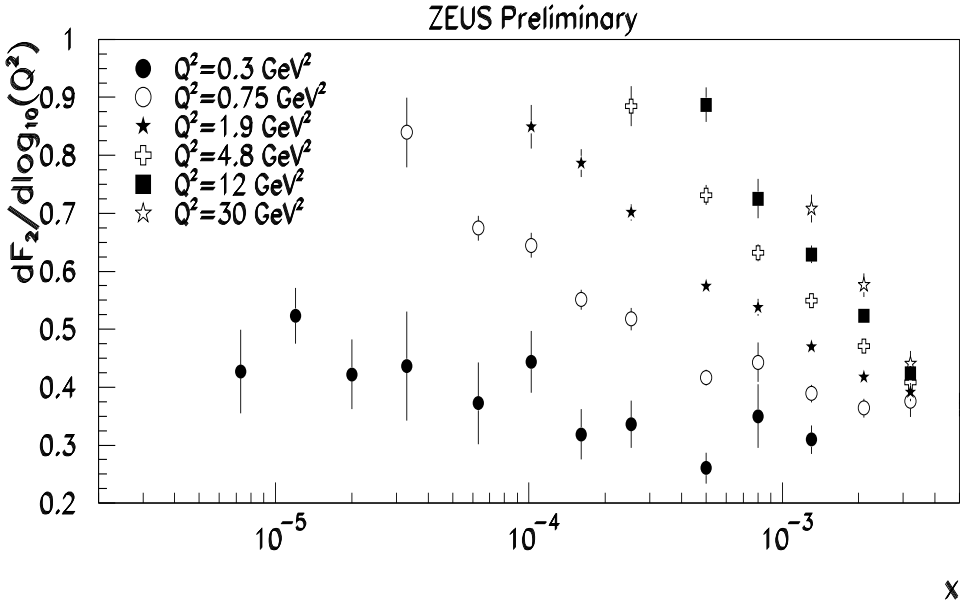


Figure 9: Measurements of the derivative $\partial F_2/\partial \log Q^2$ based on quadratic parametrizations of $F_2(x, Q^2)$ as performed recently by H1 (top) and ZEUS (bottom). The H1 data is compared with the analysis of E. Levin et al. [15] which attributes large screening corrections to the failure of the recent GRV parametrization to describe the H1 derivative data. The ZEUS data extends to lower $Q^2$ by using the data taken with the backward pipe detector. It also uses NMC and E665 data while H1 determines the derivative only in the region of H1 data.

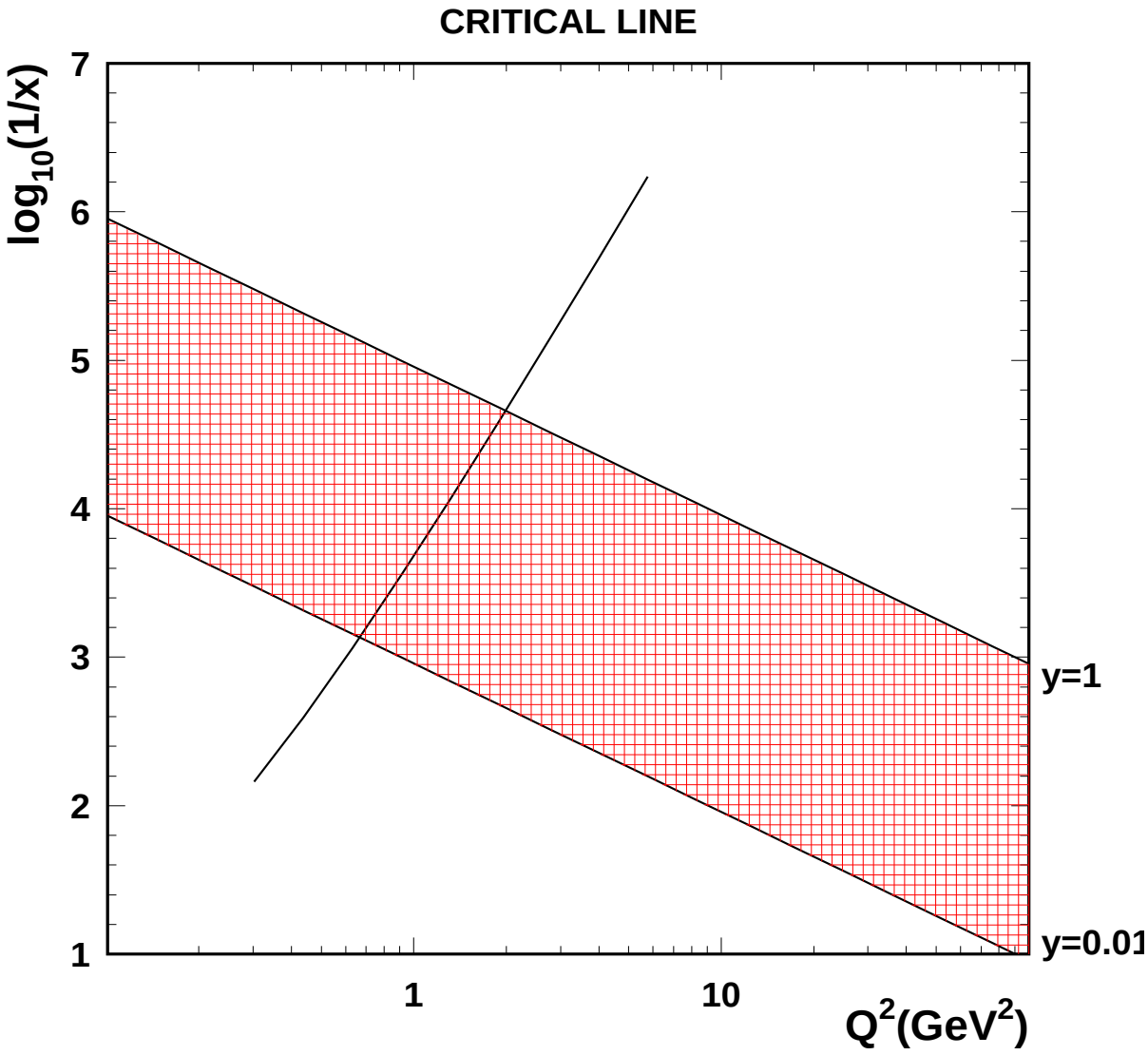


Figure 10: Critical line in the dipol saturation model. In this range the transverse size of the dipol and the proton target radius are about equal.

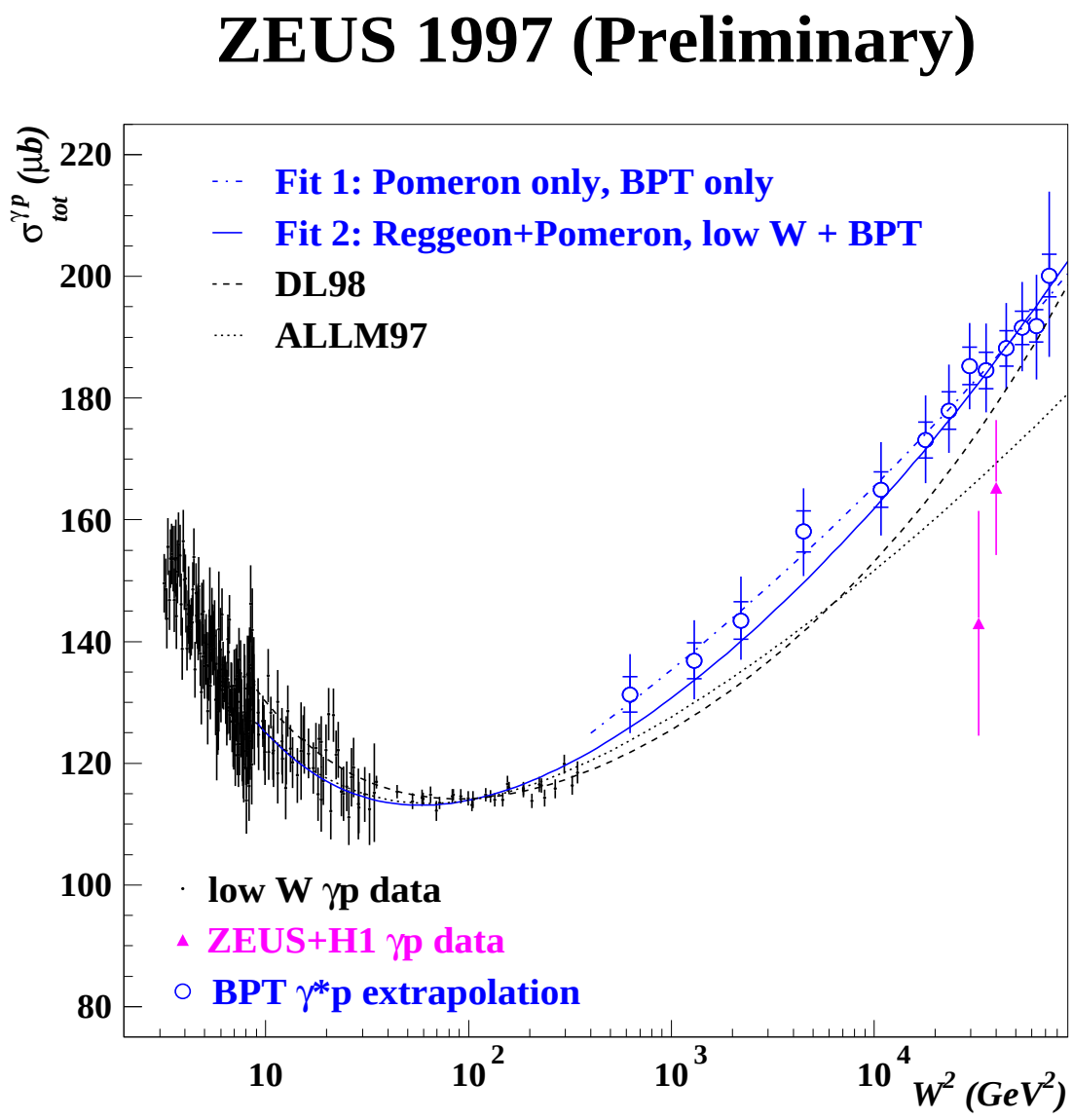


Figure 11: Extrapolated $\sigma^{\gamma^* p}_{tot}$ vs. $W^2$ compared to direct measurements and data from lower energies.

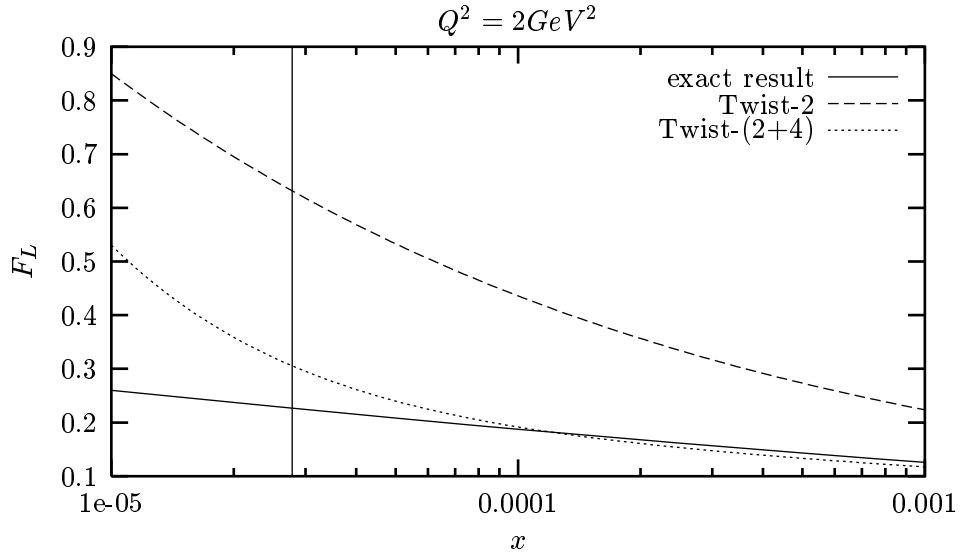


Figure 12: The longitudinal structure function and its higher twist contributions in the dipol model for $Q^2 = 2$ GeV$^2$. The vertical bar denotes the critical region ($\xi = 1$). The measurement would be placed next to this line at $x \simeq 5 \cdot 10^{-5}$.

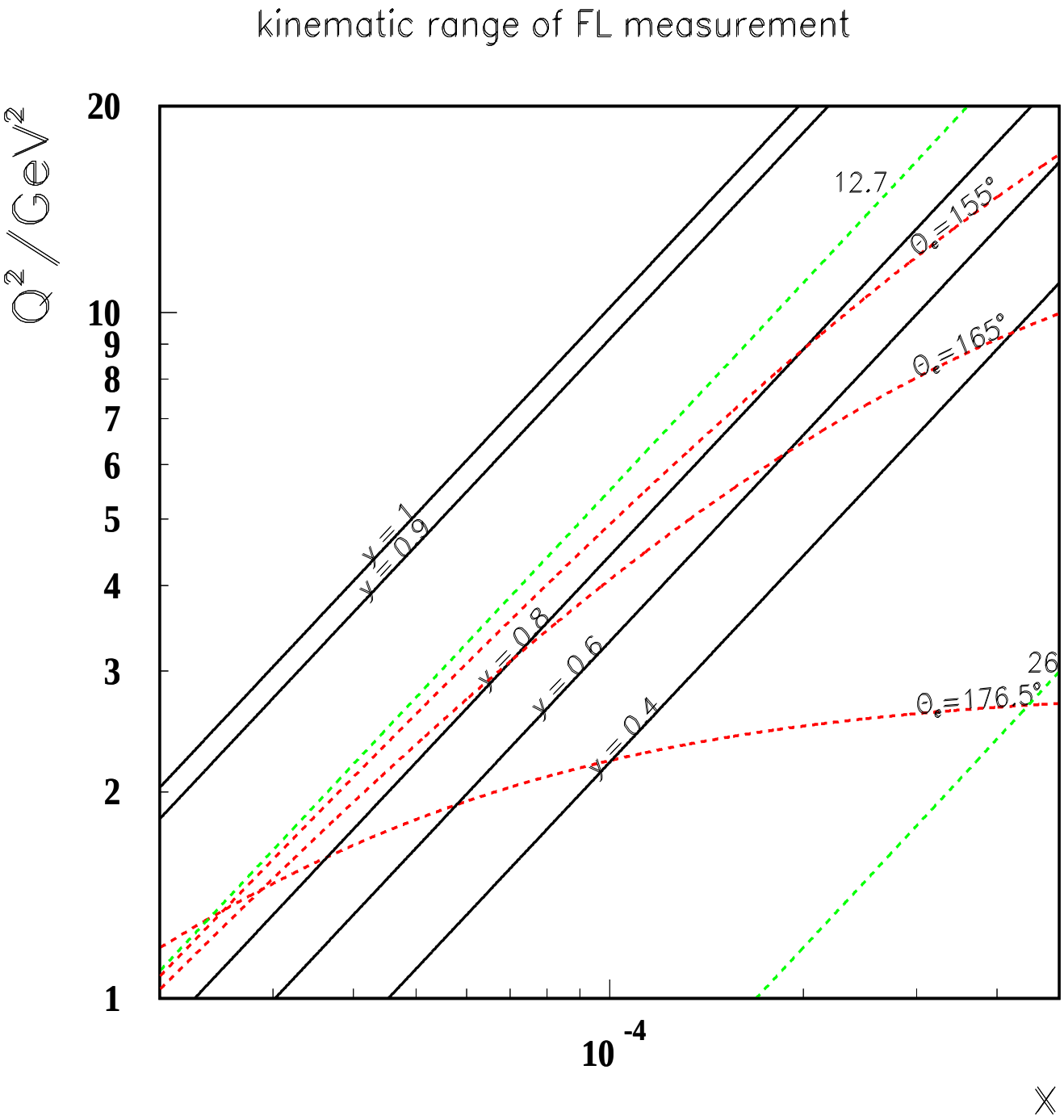


Figure 13: The kinematic range of the measurement of $F_L$ is constrained by the maximum scattering angle at 27.6 GeV ($\theta_e \simeq 176.5^o$), the minimum angle at 15 GeV ($\theta_e \simeq 155^o$) and the line of maximum accessible $y$, here drawn as $y = 0.8$ for the low energy run. With the derivative method of accessing $F_L$ the region near to $y = 0.9$ can be reached at high positron beam energy. This method can also be cross checked with the direct measurement in the high $y$ region of the low energy data.

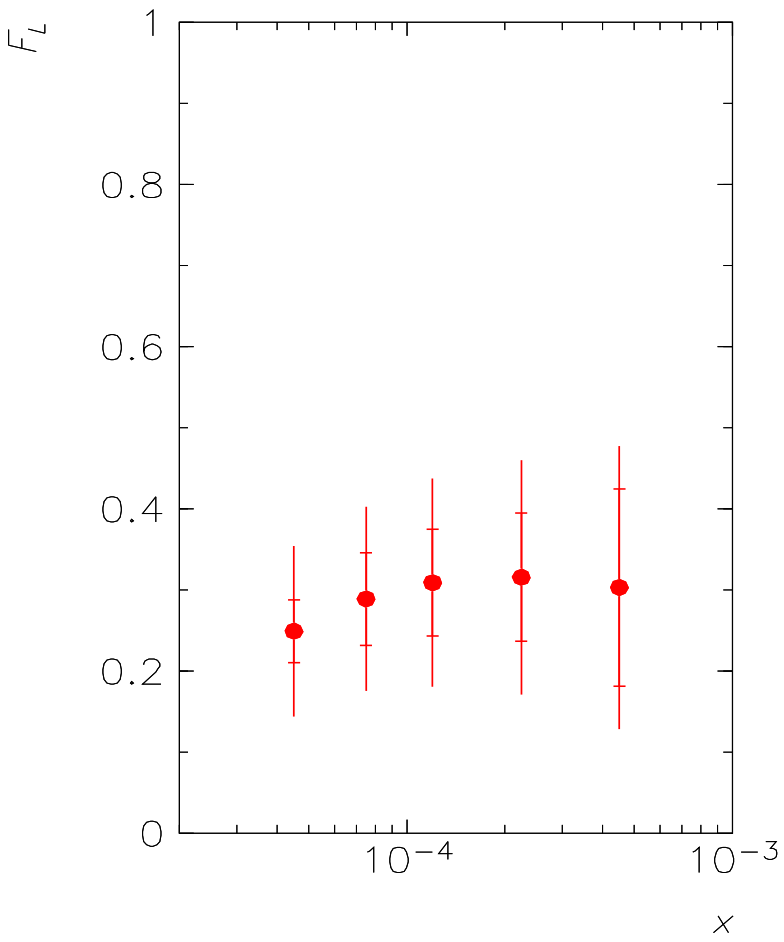


Figure 14: Simulated measurement of the longitudinal structure function assuming a systematic error ranging from 4% at $y = 0.8$ to 3% at $y = 0.5$, luminosities of 3 pb$^{-1}$ for 27.6 GeV data and 0.5 pb$^{-1}$ for 15 GeV data. The measurement is assumed to extend to $y \leq 0.8$. The points correspond to a recent parametrization of GRV. The inner error bar represents the statistical error, the full error is the systematic and statistical error added in quadrature. Due to the specific sensitivity to $F_L$, restricted to high $y$, for each $x$ point $Q^2$ varies corresponding to 2, 3, 5, 9 and 17 GeV$^2$, respectively. The data were binned in bins of constant $\nu = sy/2M_p$.

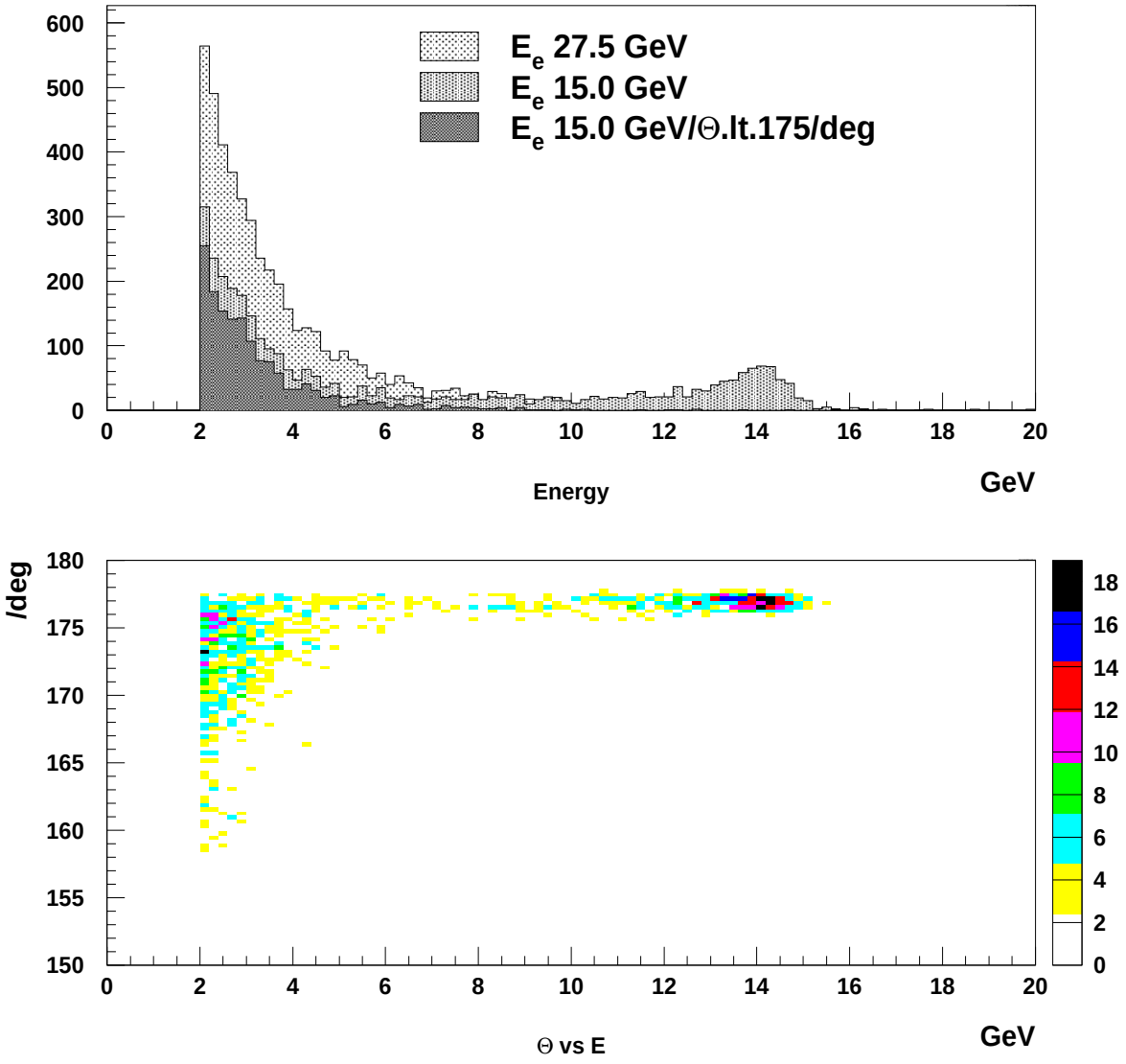


Figure 15: Simulation of photoproduction background for 27.6 GeV and 15 GeV. The upper plot shows the energy distributions for both energy settings, normalized to the same luminosity. The lower plot shows the correlation of the energy of the scattered positron candidate with the scattering angle. Since the PHOJET simulation was extended to $Q^2 = 1$ GeV$^2$ at large angles genuine scattered positrons are seen which build a kinematic peak in the energy distribution. The low $Q^2$ acceptance limit of the direct $F_L$ measurement is determined by the $\theta$ edge of the acceptance for the 27.6 GeV data, i.e. about $177^o$. This roughly corresponds to $175^o$ at 15 GeV. The effect of cutting at this angle on the energy distribution is visible in both plots.